Evolution of source attributed organic aerosols and gases in a megacity of central China

Siyuan Li [1], Dantong Liu [1,*], Shaofei Kong [2,*], Yangzhou Wu [1], Kang Hu [1], Huang Zheng [2], Yi Cheng [2], Shurui Zheng [2], Xiaotong Jiang [1], Shuo Ding [1], Dawei Hu [3], Quan Liu [4], Ping Tian [5], Delong Zhao [5], Jiujiang Sheng [5]

[1] Department of Atmospheric Sciences, School of Earth Sciences, Zhejiang University, Hangzhou 310027, China
[2] Department of Atmospheric Sciences, School of Environmental Studies, China University of Geosciences, Wuhan, 430074, China
[3] Centre for Atmospheric Sciences, School of Earth and Environmental Sciences, University of Manchester, Manchester M13 9PL, UK
[4] State Key Laboratory of Severe Weather & Key Laboratory of Atmospheric Chemistry of CMA, Chinese Academy of Meteorological Sciences, Beijing 100081, China
[5] Beijing Key Laboratory of Cloud, Precipitation and Atmospheric Water Resources, Beijing Meteorological Service, Beijing 100089, China; Field Experiment Base of Cloud and Precipitation Research in North China, China Meteorological Administration, Beijing 100089, China.

Correspondence to: Dantong Liu (dantongliu@zju.edu.cn); Shaofei Kong (kongshaofei@cug.edu.cn)

Abstract. The secondary production of the oxygenated organic aerosol (OOA) impacts air quality, climate and human health. The importance of various sources in contributing to the OOA loading and associated different ageing mechanisms remains to be elucidated. Here we present concurrent observation and factorization analysis on the mass spectra of organic aerosol (OA) by a high-resolution aerosol mass spectrometer and volatile organic compounds (VOCs) by a proton-transfer-reaction mass spectrometer in Wuhan, a megacity in central China during autumntime. The full mass spectra of organics with two principle anthropogenic sources were identified as the traffic and cooking sources, for their primary emission profiles in aerosol and gas phases, the evolutions, and their respective roles in producing OOA and secondary VOCs. Primary emissions in gas and aerosol phases both contributed to the production of OOA. The photooxidation of traffic sources from morning rush-hour caused 2.5-folds increase of OOA mass in a higher oxidation state (oxygen-to-carbon, O/C = 0.72), coproducing gas-phase carboxylic acids; while at night, cooking aerosols and VOCs (particularly acrolein and hexanal) importantly caused the nocturnal formation of oxygenated intermediate VOCs, increasing OOA mass by a factor of 1.7 (O/C = 0.42). The daytime and nighttime formation of secondary aerosols as contributed by different sources, was found to be modulated by solar radiation and air moisture respectively. The environmental policy should therefore consider the primary emissions and their respective ageing mechanisms influenced by meteorological conditions.

1 Introduction

The transformation between gas and aerosol phase of organic species produces secondary organic aerosols (SOA) (Kroll and Seinfeld, 2008; Hallquist et al., 2009; Slowik et al., 2010), which forms important global budget of aerosol loadings (Heald et al., 2005; Zhang et al., 2007), exerting climate (Poschl, 2005; Seinfeld et al., 2016) and environmental impacts (Von Schneidemesser et al., 2011; Huang et al., 2014). Given the large complexities of organic species, the yields (Goldstein and Galbally, 2007; Ortiz-Montalvo et al., 2014) and production rates (Sareen et al., 2013; Jokinen et al., 2015) of SOA from gas precursors are influenced by the diversities of source profiles (emission mass percentages among species) (Lin et al., 2012; Shrivastava et al., 2015) and environmental factors (such as radiation, air moisture and ambient temperature) (Clark et al., 2016; Li et al., 2021b; Wang et al., 2021). This raises challenges for source-oriented environmental policy making, until explicit understanding on the formation mechanism of SOA from different sources.

The application of detailed mass spectra of organic aerosols allows the online source attribution of organic aerosol (OA) (Canagaratna et al., 2007; Ng et al., 2011a), based on the factorization analysis on the mass spectra of OA which groups the covaried species from certain sources (Ulbrich et al., 2009). This factorization technique allows identification of primary sources and aged secondary sources at a receptor measurement site. The complex aerosol sources in urban environment have been commonly recognized as traffic sources mainly from vehicles on road (Zhu et al., 2021), biomass burning from open or closed combustion (Adler et al., 2011), coal combustion normally in cold season for heating (Xu et al., 2019) and more localized cooking sources (Allan et al., 2010; Zhang et al., 2020). The secondary sources are oxygenated OA which may be from oxidizing volatile organic compounds (VOCs) following condensation (Donahue et al., 2006), or heterogenous oxidation occurring on particle phase (Claeys et al., 2004). Among these sources, SOA has been found to be the main contributor of OA mass loading (41–69 %) in urban environment of East Asia (Sun et al., 2014; Hu et al., 2017), especially in warm season when primary emissions were low, along with high ambient temperature and more intensive chemical reactions (Hu et al., 2016). The formation of SOA from VOCs may experience a few reaction generations (Kroll and Seinfeld, 2008) and could interact with other sources of species during the process (Shrivastava et al., 2017), hereby complicating the goal of identifying the key precursors in contributing to the consequent SOA. In addition, some primary gases already have somehow low volatility and may not require a long reaction chain to become condensable, such as some primarily emitted intermediate volatility organic compounds (IVOCs) may substantially contribute to the SOA (Robinson et al., 2007; Huang et al., 2021). An understanding of source profiles of primary emissions in both gas and aerosol phases is therefore important to rule out the source-dependant production of SOA. The above necessitates the concurrent investigation on the compositions of gases and aerosols at a receptor site, along with their evolution and interaction, in order to elucidate the role of each source in contributing to SOA.

In this study, we performed online continuous measurements on the detailed mass spectra of organics concurrently on aerosol and gas phases, in a typical anthropogenically polluted region in central China, where such data had been rarely

64 reported. Factorization analysis is performed on the mass spectra of organics in both aerosol and gas phases, to investigate

65 the source-oriented gas-aerosol evolution and SOA formation in this region.

2 Materials and methods

66

2.1 Sampling site

67

68   The field experiment was performed in the campus of the China University of Geosciences (Wuhan) (114.40° E, 30.52°

69 N) during Oct.–Nov. 2019 (Hu et al., 2021). The site represents a typical region of mixed residential/traffic sources (Fig. S1).

70 Due to the preparation and hosting of the 7th CISM Military World Games during the experimental period, the government

71 implemented strict emission reduction measures, particularly for the industrial sources and heavy vehicle emissions in the

72 main roads. The more localized pollution sources, such as traffic emission from smaller sizes of vehicles and cooking

73 sources dominated the pollution in this study, besides those transported from surrounding regions during some heavy

74 pollution events (Zheng et al., 2019; Zheng et al., 2020). The HYSPLIT model (Draxler and Hess, 1997) with a 3-hourly 1°

75 $\times$ 1° wind field from the GDAS reanalysis products was used to obtain the 36-h backward trajectories initializing from the

76 location of the experiment site. The cluster analysis was performed to categorize the trajectories into three groups by

77 minimizing the differences in each group and maximizing the differences among groups (Moody and Galloway, 1988).

2.2 Instrumentation

78

2.2.1 Measurements of mass spectra of aerosols and gases

79

80   The mass concentration and chemical composition of NR-PM$_1$ were measured by a HR-ToF-AMS (Aerodyne Research

81 Inc., USA), including organics, nitrate (NO$_3^-$), sulphate (SO$_4^{2-}$), chloride (Chl$^-$), and ammonium (NH$_4^+$). The detailed can be

82 found elsewhere (Decarlo et al., 2006). Briefly, the aerosols are dried using a diffusion dryer before entering the AMS and

83 through a critical orifice into a narrow beam via an aerodynamic lens. The aerosol size is determined using the flight time of

84 particles to the thermal vaporization and ionization chamber. Then the aerosols are successively vaporized by a heated

85 surface (~600 ℃), ionized by electron ionization (EI, 70 eV), and detected by a mass spectrometer detector. During this field

86 observation, the HR-ToF-AMS was operated under V mode with high sensitivity. The composition-dependent collection

87 efficiencies were applied (Middlebrook et al., 2012), and the ionization efficiency was calibrated using 300 nm pure

88 ammonium nitrate (Jayne et al., 2000). Elemental analysis (EA) was also executed using the "Improved Ambient" method

89 (Canagaratna et al., 2015) to obtain the hydrogen-to-carbon ratio (H/C), oxygen-to-carbon ratio (O/C), and nitrogen-to-

90 carbon ratio (N/C).

91   The Proton-Transfer-Reactor Time-of-Flight Mass Spectrometer (PTR-ToF-MS 8000, Ionicon Analytik GmbH

92 Innsbruck, Austria) was deployed to quantify VOCs in this research. The operating and calibration of the PTR followed the

93 routine described previously (Cappellin et al., 2012; Bruns et al., 2016). Briefly, the PTR was operated with hydronium ions

94 (H$_3$O$^+$) as the reagent and with a drift tube pressure of 2.2 mbar, voltage of 600 V and temperature of 60 °C. The ratio of the

95 electric field (E) and the density of the buffer gas (N) in the drift tube, which dictates the ion drift velocity in the drift tube, is

96 135 Td. MS transmission function was performed using a mixture of VOCs (formaldehyde, methanol, acetonitrile,

97 acetaldehyde, acetone, isoprene, methyl ethyl ketone, benzene, toluene, styrene, benzaldehyde, ethylbenzene, 1,3,5-

98 trimethylbenzene). Mass calibration was done using H$_3$O$^+$ (m/z 21.0226), CH$_3$COCH$_4$$^+$ (m/z 59.0490) and monoterpenes (m/z

99 137.1290). The shift in m/z is minor which ensures that the mass calibration was sufficient for all compounds. The

100 background measurements were performed using a dry zero air cylinder. The measurement error is described in Text S2. A

101 separate reaction rate constant is applied to convert the ion signal into concentration (Bruns et al., 2016), or the default

102 reaction rate constant 2×10^{-9} cm^3 s^{-1} can be applied to all other ions (Wang et al., 2020b). The vapor saturation concentration

103 (equilibrium vapor pressures) (C^*) of each VOC compound at 25 ºC is estimated using the parameterization based on

104 elemental ratio and molecular weight (Fig. S2) (Li et al., 2016). A logC^* (in μg m^{-3}) lower than 6.5 is deemed to be

105 intermediate VOC (IVOC). According to Fig. S2, VOC species (with m/z > 120) are mainly identified to be IVOCs in this

106 study, thus the fraction of these larger molecular weight (MW) VOCs (m/z > 120) is used to evaluate the potential influence

107 of IVOCs.

108 2.2.2 PMF analysis on the mass spectra of OA and VOCs

109 Positive matrix factorization (PMF) (Paatero and Tapper, 1994) was performed on the high-resolution organic mass

110 spectral matrix of OA (Ulbrich et al., 2009; Decarlo et al., 2010). In this work, m/z > 120 and isotopic ions were excluded in

111 PMF analysis due to the limited mass resolution and low contributions to OA loading (~5 %). After a careful evaluation of

112 the mass spectral profiles and correlations with time series of tracers, diurnal variations, four OA factors from total OA were

113 identified with $f$peak = 0, including hydrocarbon-related OA (HOA), cooking OA (COA), low-oxidized oxygenated OA

114 (LO-OOA, OOA1), and more-oxidized oxygenated OA (MO-OOA, OOA2). The detail of PMF diagnostic was summarized

115 in Text S1 and Fig. S3.

116 The EPA PMF 5.0 model (Paatero and Tapper, 1994) was used for the source apportionment of VOC species. The 109

117 VOCs were used for the PMF analysis. The uncertainties from each sample were determined according to the method

118 detection limit (MDL) and the error fraction (%). The detail of PMF diagnostic was summarized in Text S2 and Fig. S4. Five

119 factors were ultimately selected, and the Q/Q_{exp} ratio was 0.96 on average (Fig. S4). The rotation ambiguity was explored by

120 varying the $f$peak values from -3 to +3, and the results with $f$peak = 0 were selected for the lowest dQ (robust), indicating the

121 stability of the PMF solution (Zhou et al., 2019). Most of the residuals are distributed normally, ranging from -3 and +3,

122 suggesting the model fits the data well.

123 2.2.3 Other measurements

124 The concentration of BC particles was measured by a single particle soot photometer (SP2, DMT Inc.). The operation

125 and data analysis procedures of the SP2 have been described elsewhere (Schwarz et al., 2008; Liu et al., 2010). The SP2

126 incandescence signal was calibrated for refractory BC (rBC) mass using the Aquadag black carbon particle standards

127 (Acheson Inc., USA) and corrected for ambient rBC with a factor of 0.75 (Laborde et al., 2012).

128 The size distribution and number concentration of aerosols with an electrical mobility diameter from 12 to 552 nm were

129 also measured by a scanning mobility particle sizer (SMPS, Model 3081, impactor 50 % cut off at 0.677 μm; CPC model

130 3775 at a flow rate 0.3 L min^{-1}). PM$_1$ mass concentration calculated based on the volume concentration measured by the

131 SMPS agreed well with that from the sum of compositions by the HR-ToF-AMS and SP2 (r = 0.71, slope = 0.90).

132 The gas-phase species including NO$_x$, O$_3$, and CO were measured in real time by a series of Wuhan Tianhong analyzers

133 (TH-2001H, TH-2003H, TH-2004H, respectively). These instruments were calibrated periodically with the corresponding

134 standard gas to ensure the accuracy of the observation data. In addition, the meteorological parameters including temperature

135 (T), relative humidity (RH), and wind speed and direction were recorded by an automatic weather station.

136 3 Results and discussion

137 3.1 Chemical compositions of PM$_1$

138 The time series of mass concentrations of BC, non-refractory-PM$_1$ (NR-PM$_1$) species (i.e., OA, SO$_4^{2-}$, NO$_3^-$, NH$_4^+$, and

139 Cl$^-$) and their relative contributions are summarized in Fig. 1. During this field observation, the mass concentrations of NR-

140 PM$_1$ were in the range of 2.5–44.8 µg m^{-3}, with an average of 12.7 ± 5.7 µg m^{-3}, which is close to those observed in the

141 North China Plain in autumn 2019 (15.1 µg m^{-3}) (Li et al., 2021a), and was much lower than that (41.3 ± 42.7 µg m^{-3})

142 observed in Beijing in autumn 2012 (Hu et al., 2017). The mean mass concentration of BC was 0.29 ± 0.17 µg m^{-3} with the

143 range of 0.1–1.0 µg m^{-3}. Among all species in NR-PM$_1$, OA contributed the major (49.2 %), indicating the dominant role of

144 OA in autumntime of PM$_1$ pollution in this region. Inorganic aerosol accounted for 50.8 % of NR-PM$_1$ in which sulphate

145 was the largest contributor (21.5 %), followed by nitrate (18.5 %), ammonium (10.7 %), and chloride (0.1 %), which has

146 similar relative contributions to those observed in field (Chen et al., 2021). The number concentration of all particles peaked

147 at 95 ± 38 nm in with regular growth during every field day. Fig. 1 also presents the temporal evolution variation in

148 meteorological parameters. During the field observation period, the average temperature and relative humidity (RH) were

149 19.3 ± 3.6°C (11.2–29.4 °C) and 75.0 % ± 17.5 % (25.0–99.0 %), respectively. The O$_3$ concentration with an average of 30.7

150 ± 13.0 ppb, was highest 54.5 ppb at 15:00, likely due to the high temperature and enhanced photochemical processing

151 (Zheng et al., 2021).

152 Fig. 1f shows the spatial distribution of aerosol optical depth (AOD) and 36 h backward trajectories during the

153 campaign. Cluster-1 (C1) shows the circulated air mass with shortest transport distance for the past 36 h (36 % fraction); C2

154 is the northerly transported air mass (55 % fraction), over regions with higher AOD; C3 is the most rapid transport through

155 the northeast China and some coastal areas. It therefore separates the periods with more local air mass or influences from
156 regional transport. Fig. 1g shows the diurnal variations of solar radiation and RH, peaking in the day and night respectively.

157
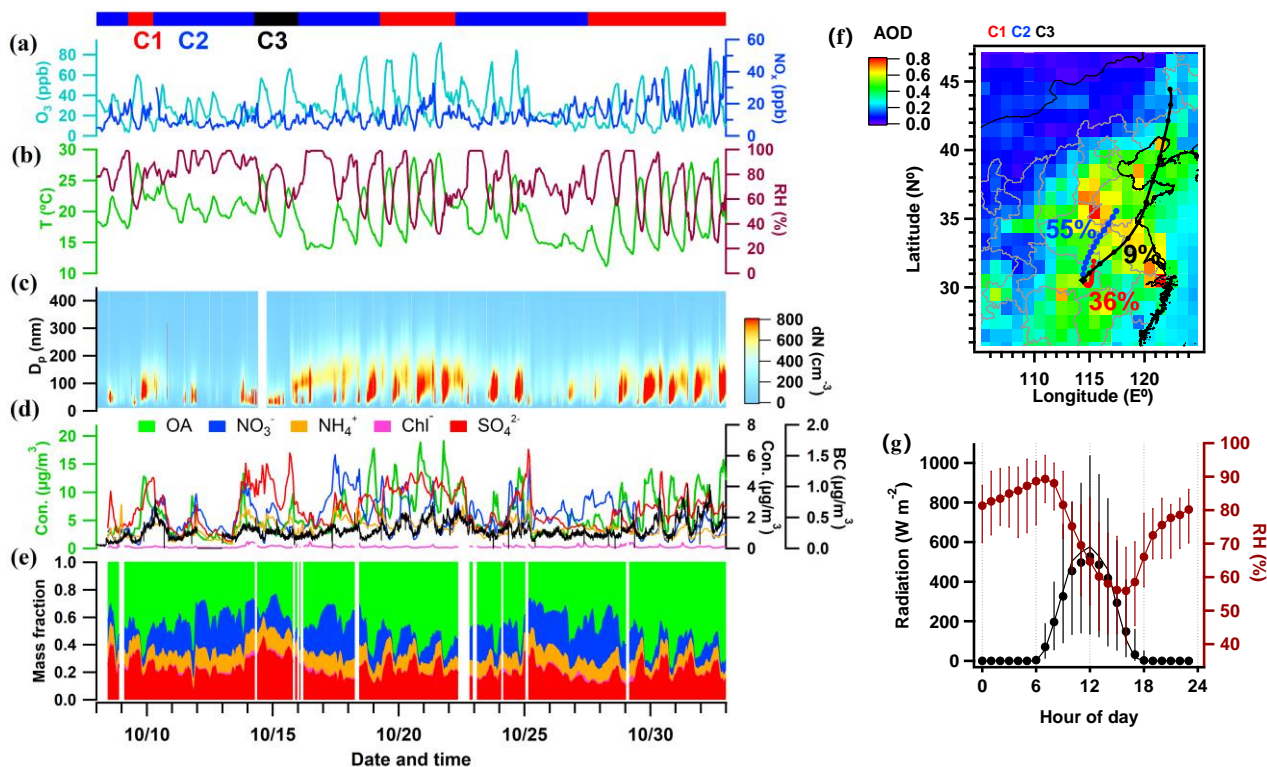
Figure 1: Time series of (a) mass concentrations of O_3 and NO_x; (b) ambient temperature (T) and relative humidity (RH); (c) number size distribution measured by the SMPS; (d) mass concentrations of key aerosol species (the green left y-axis represents OA, the right y-axis represents other aerosol species); (e) mass fractions of chemical species in non-refractory PM_1; (f) spatial distribution of mean aerosol optical depth (AOD) during the experiment and the clustered 36 h backward trajectories; (g) diurnal profiles of direct solar radiation and RH.

163 **3.2 Source attributed organic aerosol**

164   The resolved OA factors by the PMF analysis on the AMS measurements are shown in Fig. 2. The first factor is
165 characterized by prominent hydrocarbon ion series of $C_nH_{2n-1}^+$ and $C_nH_{2n+1}^+$ (Fig. 2a), with a low O/C ratio (0.24), which is
166 generally considered to be related to the emissions of fossil fuel combustion and vehicle emissions (Huang et al., 2010;
167 Morgan et al., 2010; Ng et al., 2011b). The time series of the factor correlated well with NO_x (r = 0.71) and BC (r = 0.83)
168 (Fig. 2e and Table S1). The diurnal pattern of this factor showed peaks in the morning and afternoon rush-hour (Fig. 2i),
169 with a major increase from 5:30, reaching a peak value of 1.5 µg m^{-3} at 8:30. The concentration gradually decreased around
170 noontime due to boundary layer dilution until 15:00 and reached a minimum of 0.6 µg m^{-3}. This spectrum also contained
171 some fragment markers for possible coal combustion OA (CCOA), i.e. $C_9H_7^+$ (*m/z* 115, r = 0.73) (Hu et al., 2013). This

172 factor was not distinctly resolved in this dataset maybe due to the urban nature of the site, where the traffic source may have

173 overwhelmed, due to the less significant coal combustion pollutants during the sampling period.

174   The second factor was characterized by m/z 55 ($C_4H_7^+$, $C_3H_3O^+$) and 57 ($C_4H_9^+$, $C_3H_5O^+$), accounting for 10 % and 3.5

175 % of the total spectrum, respectively (Fig. 2b), with the lowest O/C ratio among factors (0.16). This factor has a

176 $C_3H_3O^+/C_3H_5O^+$ of 3.0 and $C_4H_7^+/C_4H_9^+$ of 2.0 (1.0 is usually for HOA), indicating it as cooking source rather than HOA

177 (Mohr et al., 2012). The correlation coefficient of the COA factor and marker fragment $C_6H_{10}O^+$ was 0.91, which is also

178 similar to a previous study (Sun et al., 2011). The diurnal pattern of this factor showed a major peak during 18:00–20:00,

179 reaching up to 4.0 µg m^{-3} on average, in addition to a smaller peak at lunch time, which corroborated the diurnal cooking

180 activities. Previous studies reported COA accounted for 6.5–30 % of the total OA in urban (Rogge et al., 1991; Lanz et al.,

181 2008; Allan et al., 2010; Xu et al., 2014). Here the concentrations of COA in OA were in the range of 0.5–4.5 µg m^{-3} and

182 accounted for 23 % of OA mass fraction on average. The cooking emission in the studying region was likely from charcoal-

183 grilling activities, which was popular in the surrounding areas.

184   Besides the two primary OA, additional two oxygenated OA (OOA) factors are identified. According to the oxidation

185 state, OOA was separated into lower (OOA1) and more oxidized (OOA2) factors. OOA1 factor contained abundant oxygen-

186 containing fragments, accounting for more than 50 % of the total mass spectrum, with an O/C of 0.42. In particular, the

187 oxygenated fragment containing one oxygen accounted for 39 %. The $C_2H_3O^+$ ion (m/z 43) is an important component of less

188 oxidized SOA (Wang et al., 2020a), which was highly correlated with OOA1 (r = 0.94). OOA1 showed lower concentration

189 during daytime but higher concentration during nighttime (Fig. 2k). Such diurnal variation was similar to that of RH (r =

190 0.45), but opposite to that of solar radiation, which was similar to a previous report (Sun et al., 2014). OOA1 may thus be

191 associated with aqueous reactions when high RH. The co-occurrence of nighttime peak of OOA1 and COA suggested the

192 primary source of cooking emission may have considerably contributed to the production of OOA1.

193   The factor OOA2 had the highest O/C of 0.72 and contained 61 % oxygen-containing fragments (Fig. 2d), which is very

194 similar to the spectra of OOA factor resolved in other cities (0.60 and 67 % in Mexico City, 0.80 and 66 % in Pasadena)

195 (Aiken et al., 2009; Hayes et al., 2013). This factor was correlated strongly with the fragment of CO_2^+ (r = 0.79). Compared

196 to OOA1, this factor showed obvious diurnal variations with a major enhancement at around noontime (10:00–15:00), up to

197 2.9 µg m^{-3}, indicating the photochemical production of SOA during daytime. The variation of OOA2 correlated with odd

198 oxygen (O_x = O_3 + NO_2, r = 0.70), agreeing with previous observations that oxidized OA had strong correlation with O_x

199 (Wood et al., 2010; Hu et al., 2016). Considering the high RH during the experiment (> 60 %, Fig. 1g), OOA2 factor may

200 have also experienced aqueous chemistry and showed good correlation with sulphate (r = 0.82).
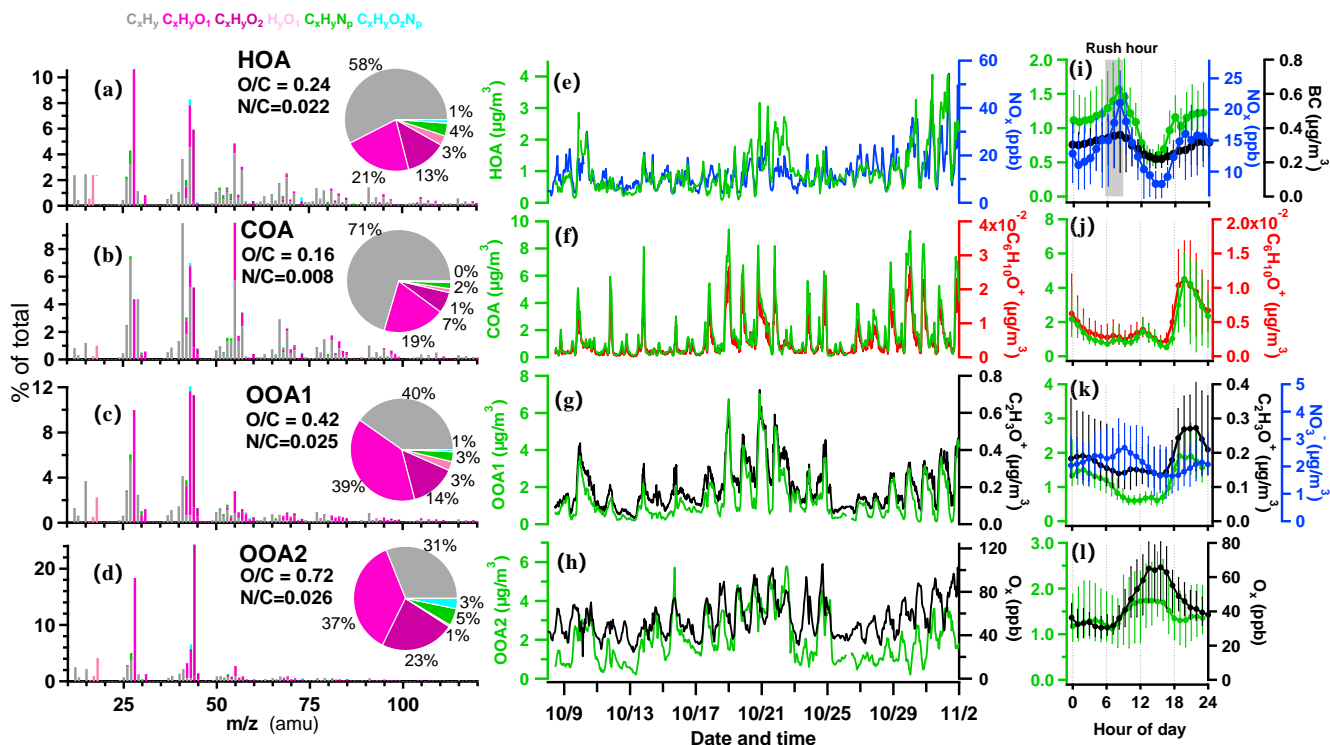
Figure 2: Results of source-attributed organic aerosols by the PMF analysis on the OA mass spectra measured by the HR-TOF-AMS. Mass spectra of PMF factors for (a) hydrocarbon-like OA (HOA); (b) cooking OA (COA); (c) oxygenated OA1 (OOA1); (d) oxygenated OA2 (OOA2). The pies show the relative contributions of the six ion categories to each factor. (e-h) Temporal variations of four OA factors (HOA, COA, OOA1 and OOA2) with each correlated species as NO_x, $C_6H_{10}O^+$, $C_2H_3O^+$ and O_x. (i-l) Diurnal profiles of NO_x, BC, $C_6H_{10}O^+$, $C_2H_3O^+$, NO_3^- and O_x. The lines and whiskers denote the median, the 25th and 75th percentiles at each hour, respectively.

3.3 Source attributed VOCs

Fig. 3 and Fig. S5 summarize the source attributed of VOCs and key indicators. Two primary and three secondary VOC factors were identified. Here 109 species of VOCs from the PTR-TOF-MS were used, which are mostly oxygenated or contain cyclic functional groups, in contrast with the GC-MS measurement which contains many aliphatic hydrocarbon compounds and usually only decades of species were used for the PMF analysis (Zheng et al., 2021). These may lead to some unsolved primary VOC sources for the current analysis using the PTR-measured VOCs, if the source contained crucial markers of aliphatic species, but this method may have great advantage in comprehensively resolving factors of secondary VOCs. This may explain the less primary but more secondary VOC factors compared to conventional PMF-resolved VOC sources (Cai et al., 2010).

The first factor was dominated by aromatic compounds, such as C_6H_6 (*m/z* 79.054) and C_7H_8 (*m/z* 93.070) in Fig. 3a. They were well established markers for vehicle emissions (Gkatzelis et al., 2021) and had a good correlation with this factor (r = 0.97 and 0.63, respectively Fig. S6). This factor showed peaks in the morning and afternoon rush-hour (Fig. 3k) and was

well correlated with HOA and NO_x (r = 0.63 and 0.53 Table S1). The concentration of this factor had a major increase during the early morning, reaching a peak value of 12.1 ± 1.3 ppb at 08:30, further corroborating the traffic source of this factor. The concentration decreased around noontime until 15:00 because of the dilution by well-developed boundary layer and in addition to its consumption through photochemical reaction due to intense solar radiation. The diurnal pattern was also high at night, although the peak was lower than early morning, the average concentration was higher by a factor of 2 than daytime. This suggests that traffic VOCs is more likely to participate in photochemical reaction, and other primary emissions may be precursors for nocturnal chemistry.

The second factor contained abundant aldehydes such as C_3H_4O (acrolein), $C_3H_6O_2$ (hydroxyacetone), $C_6H_{12}O$ (hexanal), and $C_7H_{14}O$ (heptanal) at *m/z* 57.069, 75.044, 101.096, and 115.112, respectively, as well as C_8H_{10} (C8-aromatics) and C_9H_{12} (C9-aromatics) at *m/z* 107.086 and 121.101 in VOC mass spectra (Fig. 3b), which are footprint VOCs identified from primary cooking emissions during the charbroiling and frying (Klein et al., 2016). This factor had similar time series (Fig. 3g) with COA and had high correlation (r = 0.67, Table S1). The concentration of this factor decreased during the daytime and increased after 18:00 with a peak value at 19:00 (17.2 ± 3.0 ppb). As shown in Fig. 3l, the diurnal concentration decreased strongly after emission and continued to decline throughout the night, suggesting that cooking VOCs may be major precursors and were consumed during night.

Besides the two primary VOCs, three secondary oxygenated VOCs (SecVOCs) factors are identified. These three factors are not well correlated with any primary factors attributed by the OA, are thus considered to be mainly contributed by secondary production. The daytime biogenic emission, e.g. isoprene, may also contribute to the SecVOC2 formation by interacting with OH in the presence of NO_x (Lin et al., 2013), producing methacrylic acid epoxide (MAE) and methacrolein (MACR) as intermediately involved in SOA formation (Gu et al., 2021). This factor was thus also contributed by this primary source. SecVOC2 contributed a large fraction of $C_2H_4O_2$, $C_3H_6O_3$ and $C_4H_6O_3$ (Fig. 3c), which were gas-phase carboxylic acids, the oxidation products from photochemical processes (Hartikainen et al., 2018; Li et al., 2021b). SecVOC2 had one clear peak at 13:00 (14.7 ± 2.8 ppb Fig. 3m). The time series of SecVOC2 correlated well with OOA2 (r = 0.67), following the variation of solar radiation. It had a rapid enhancement starting from 07:00 to 12:00 and declined continuously after 13:00. This indicated that many of these species can be formed rapidly during daytime and may have a short lifetime owing to the partitioning to the condensed phase and forming SOA.

SecVOC1 factor featured with some less-oxygenated VOCs e.g., $C_2H_2O_2$, $C_6H_{10}O_2$ and $C_{10}H_{14}O$ (Fig. 3d). This factor had a peak at 19:00 which was consistent with the primary cooking VOCs factor, but also increased throughout the night, peaking at midnight. This factor had a similar temporal trend with OOA1 (r = 0.76, Fig. 3i), which was less oxygenated than photochemistry dominated OOA2. Combining the features above, SecVOC1 tended to be contributed by some immediately reacted species from emissions in the late afternoon and early night. A particular factor (Fig. 3e) is significantly composed of large molecular weight (large-MW) oxidized VOCs, i.e. the mean contribution of ionic compounds with m/z > 120 was above 50 % in this factor (Fig. S5e), which was much higher than that in SecVOC2 (Fig. S5c). Fig. 3e shows its signature

253 compounds of $C_8H_{14}O$, $C_6H_{12}O_3$ and $C_8H_4O_3$, and some are nitrogen-containing VOCs, such as $C_6H_5NO_3$ and $C_8H_9NO_3$.

254 These VOCs with m/z > 120 tend to be intermediate-volatility organic compounds (IVOCs) as the estimated vapor saturation

255 concentration ($\log_{10}C^*$, 298 K) is less than 6.5 μg m^{-3} (Fig. S2). This factor is hereby termed as large-MW VOCs to indicate

256 the fraction of IVOCs, which only require few oxidation steps to become semi-volatile (Robinson et al., 2007). Fig. 3o

257 shows an increase of this factor at mid-night, later than the peak of SecVOC1, which may imply the ageing process in

258 producing these VOCs.

259
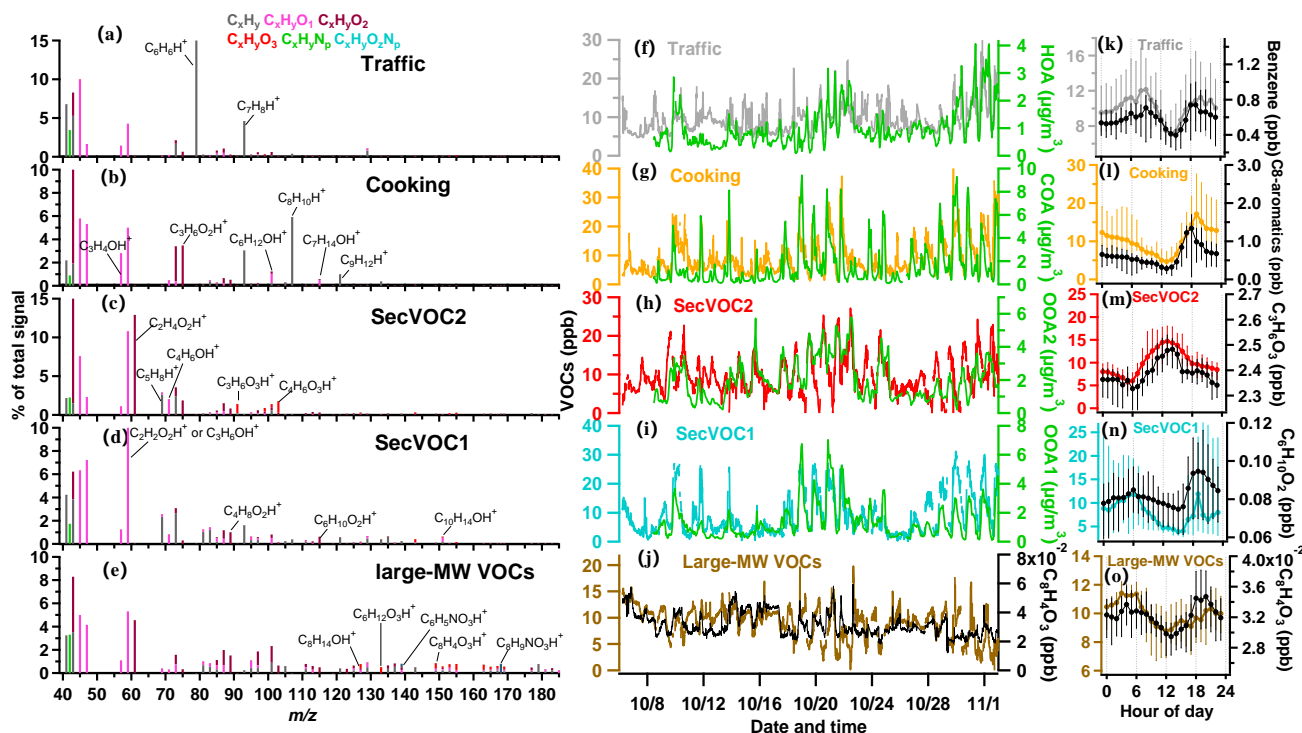
260
261 **Figure 3. Source attributed VOCs by the PMF analysis measured by the PTR-TOF-MS. (a-e) Mass spectra of the five factors**
262 **(traffic VOCs, cooking VOCs, secondary VOCs (SecVOC2, SecVOC1) and large molecular weight (MW) VOCs (large-MW**
263 **VOCs), with major fingerprint peaks labelled in the mass spectra. (f-j) Temporal variations of the five VOCs factors and their**
264 **respective correlated OA species. (k-o) Diurnal profiles of the VOC factors and their respective signature species. The lines and**
265 **whiskers denote the median, the 25th and 75th percentiles at each hour, respectively.**

266 **3.4 Oxidation process of organics in the day and night**

267   After source attribution of organics in aerosol and gas phase, we are able to identify the emission structure of primary

268 sources and the consequent evolution. Given the identified primary traffic and cooking sources were emitted in the day and

269 late afternoon respectively, this provides the potential opportunity to study the evolution of different primary sources in the

270 potentially contrasting ageing mechanisms in the day and night.

271   Fig. 4a-d shows the temporal evolution of the key factors in a week to reflect the day and night ageing. The O/C ratio in
272 the day was higher than that at night by 0.2 (Fig. 4a), corresponding with the increase of highly oxygenated fragments of
273 AMS f_{44} (CO_2^+) in the day (Fig. 4b). During night, the O/C ratio increased with the increase moderately oxygenated fragment
274 f_{43} ($C_2H_3O^+$). The diurnal variation of atomic ratio O/C of OA (Fig. 4e) showed a slight decrease at morning rush-hour and
275 sharp drop at 18:00 (by 0.2) due to the significant contribution of the traffic and cooking sources respectively, corresponding
276 with the two steps of increase at each time. This variation of O/C clearly showed the daytime and nighttime ageing processes
277 of OA for different primary sources. Notably, the O/C showed peak value of 0.54 at 15:00, implying the importance of
278 photooxidation in producing highly oxygenated OA.

279   Considering the diurnal pattern of anthropogenic activities, the traffic emission at rush-hour is deemed to be the major
280 source in contributing to the daytime production of OOA. The ratio OOA2/HOA is thus used to indicate the daytime
281 oxidation of OOA. As Fig. 4d and 4f showed, OOA2/HOA had a clear peak during daytime, and increased after 8:00 and
282 peaked at 14:00. After 15:00, the ratio gradually decreased to minimum at 20:00 and maintained to be low throughout the
283 night. This clearly demonstrated the photooxidation in producing OOA2 from oxidizing HOA. Fig. 4c and 4g give a few
284 examples of photooxidation in gas phase: the toluene showed a production of $C_3H_6O_3$ (hydroxypropionic acid) and $C_4H_6O_3$
285 (acetic anhydride) by a factor of 2 in 3 hours (Fig. S7c); the C_3H_4O (acrolein) produced the oxidized product $C_2H_2O_2$
286 (glyoxal) by a factor of 1.3 (Fig. 4h). All of these reacted species are from traffic VOCs and the corresponding products are
287 from SecVOC2. The daytime biogenic emission, e.g. isoprene, may also contribute to the SecVOC2 formation by interacting
288 with OH in the presence of NO_x (Lin et al., 2013), producing methacrylic acid epoxide (MAE) as intermediately involved in
289 SOA formation, where a considerable nitrogen content was also found in the OOA2 factor (N/C = 0.026). Overall, the highly
290 oxidized OOA2 (O/C = 0.72) is considered to be mainly contributed by the traffic source, via the oxidation of VOCs and
291 partitioning to condensed phase, direct oxidation on HOA through heterogenous oxidation (Guo et al., 2020), or VOCs
292 evaporated from HOA and further condensation after oxidation (Zhao et al., 2015). All factors may have contributed to the
293 daytime production of OOA2.

294   The nocturnal oxidation is mainly contributed by the sources emitting from late afternoon throughout the midnight.
295 Both traffic and cooking sources contributed to the emission since late afternoon, with cooking source as the predominant
296 contributor in both aerosol (Fig. 2j) and gas (Fig. 3l) phases. The ratio between the nighttime OOA1 and cooking aerosol
297 (OOA1/COA) is therefore used to indicate the nocturnal oxidation of SOA (Fig. 4d and j). There was a sudden increase of
298 OOA1/COA during the daytime because COA was consumed rapidly in the afternoon after a small amount of emission at
299 noon (Fig. 2j). The lowest OOA1/COA at 0.5 corresponded with the fresh cooking emission at 18:00, and kept increasing
300 until peaking in the early morning at 6:00 up to 3, which was an increase by a factor of 6 compared to the minima (Fig. 4j).
301 In addition to evidence for daytime reaction, Fig. 4h and Fig. S7d also gave evidence for certain reacted species during the
302 ageing at nighttime. The first-generation oxidation products from acrolein (ACR $C_3H_4OH^+$, m/z 57.033) are glyoxal
303 ($C_2H_2O_2$, m/z 59.036) and formaldehyde ($HCHOH^+$, m/z 31.018) according to the database in Master Chemical Mechanism

304   (MCM). This night oxidation is also evidenced by the formation of some nitrated organic compounds and ketone

305   compounds, such as $C_6H_5NO_3$ (nitrophenol, NP, Fig. 4l) and $C_6H_{10}O_2$ (hexanedione, Fig. 4k) produced from phenol (C_6H_6O)

306   and hexanal ($C_6H_{12}O$), respectively. Notably, an important fraction of large molecular weight-VOCs (which are mostly

307   intermediate VOCs, Fig. S2) peaked at 3:00–4:00 (Fig. 3o), consistent with the variation of OOA1/COA during night. Some

308   of these nitrated and oxygenated IVOCs may have been further oxidized and partitioned to aerosol phase, contributing to the

309   OOA1. Given the larger molecular usually has a lower O/C ratio (Hatch et al., 2017) (because of a higher content of carbon),

310   this may explain the lower O/C observed for nighttime formed OOA1 (O/C = 0.42), than OOA2 produced by daytime

311   photooxidation (O/C = 0.72). Notably, nighttime SOA had a high N/C (0.025), implying the $NO_3\cdot$-initiated from cooking

312   emissions oxidation, which was different from the organic nitrate formation mechanism during the daytime.
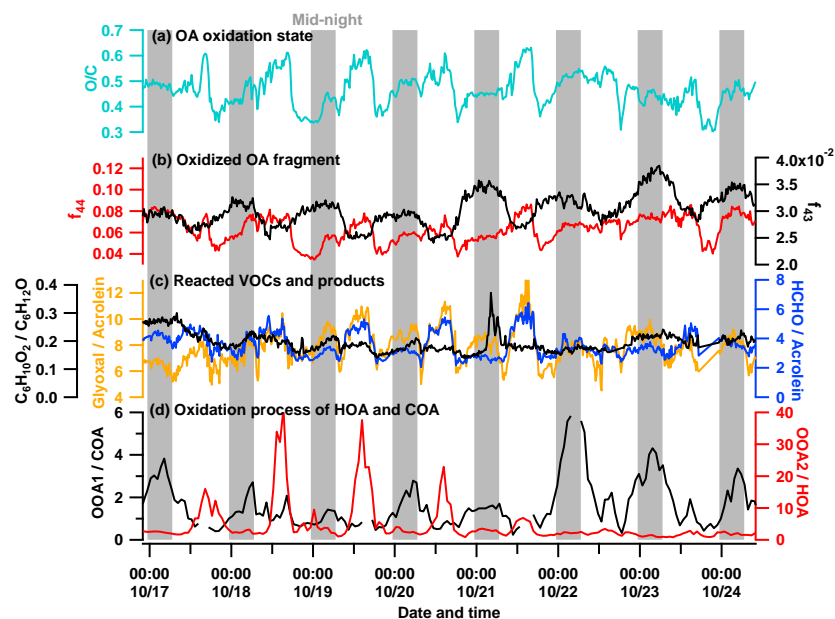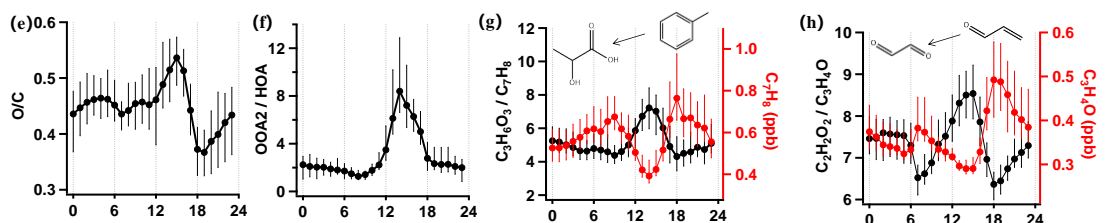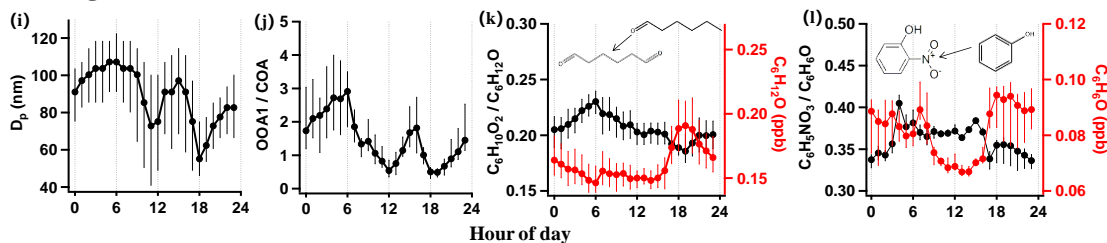
313

314 **Figure 4.** Time series showing the ageing of aerosols and gases, with grey vertical bars denoting nighttime (00:00–06:00), (a) the
315 oxygen to carbon ratio (O/C); (b) the fragment fraction at m/z 44 (f_{44}), m/z 43 (f_{43}); (c) concentration ratio of $C_6H_{10}O_2$ to $C_6H_{12}O$
316 (hexanedione to hexanal), glyoxal to acrolein, and formaldehyde to acrolein; (d) concentration ratio of OOA1 to COA and OOA2
317 to HOA. Diurnal variations of key species showing the daytime photooxidation and nighttime oxidation, (e) ratio of O/C; (f) ratio
318 of OOA2 to HOA; (g) concentration of C_7H_8 and ratio of $C_3H_6O_3$ to C_7H_8 (hydroxypropionic acid to toluene); (h) concentration of
319 C_3H_4O and ratio of $C_2H_2O_2$ to C_3H_4O (glyoxal to acrolein); (i) particle diameter (D_p); (j) ratio of OOA1 to COA; (k) concentration
320 of $C_6H_{12}O$ and ratio of $C_6H_{10}O_2$ to $C_6H_{12}O$ (hexanedione to hexanal); (l) concentration of C_6H_6O and ratio of $C_6H_5NO_3$ to C_6H_6O
321 (nitrophenol to phenol).

322

323   Fig. 5 summarizes the key indicators for the contrasting daytime and nighttime oxidation process. The concentrations
324 are normalized by ΔCO, where ΔCO is the total CO concentration subtracted by the background concentration (1th

percentile of the dataset), to indicate the variation of species regardless of the boundary layer evolution, wind speed, wind direction and temperature (Gouw and Jimenez, 2009). The odd oxygen O_x ($O_3 + NO_2$) has been widely used to generally indicate the activity of daytime photochemistry (Hu et al., 2017), and the enhanced moisture is the main driving factor for nighttime chemistry. The O_x concentration and RH are therefore used as references with which the variations of species were correlated in the day and night, respectively. As Fig. 5a showed, the traffic primary emissions in both gas (traffic VOCs) and aerosol phase (HOA) declined with increased O_x by 60 % and 40 % respectively, suggesting their roles as precursors in the daytime reaction. The produced species are oxygenated SecVOC2 and OOA2, showing enhancement with O_x, peaking at midday-afternoon. This process was rapid as the SOA production by a factor of 2.5 and the oxygenated VOCs production by a factor of 1.7 within 6 hours. The traffic VOCs are widely observed to contribute to SOA production, with aromatic compounds serving as key precursors (Fang et al., 2021). The semi-volatile nature of HOA means it could be evaporated to gas phase and further oxidized to recondense as SOA (Robinson et al., 2007). The decrease rate of HOA with increased photochemical age was also found in urban environment (Zhu et al., 2021), generally consistent with the reaction rate in this study. Here we linked the declining rate as a function of photochemical activities for both reacted aerosol and gas phases for traffic sources. The gases evaporated from aerosol phase (especially under higher temperature when increased saturation pressure for semi-volatile or intermediate volatile species) and primary VOCs may be simultaneously involved in the photooxidation, further contributing to the SOA formation.

For nocturnal oxidation shown in Fig. 5b, the reacted species are cooking VOCs and COA (decrease by 35 % and 77 %, respectively), producing SecVOC1 and large-MW oxygenated VOCs, with an increase of night SOA formation by a factor of 1.7. The nocturnal processes may have largely involved aqueous reactions, because the variations of reacted or produced species were highly correlated with RH (r > 0.95, Fig. 5b). The large-MW VOCs (mostly IVOCs) increased by 50 % and reached maxima when highest RH. This suggests the moisture may have been involved in converting some primary VOCs to IVOCs, which further contribute to the SOA production during nighttime. Previous studies also found the oxidation of IVOCs from cooking sources can be an important source of SOA (Zhang et al., 2020). The evidence is given here that organic aerosols and gases from cooking emission had been reacted and contributed to SOA. An approximate production rate of 0.2 µg m^{-3} h^{-1} of OOA from cooking source can be obtained by considering the ageing time of ~10 h (from COA peak 18:00 to OOA1 peak 4:00), which was generally consistent with previous laboratory work using gas precursors from cooking sources (0.07–0.5 µg m^{-3} h^{-1}) (Liu et al., 2017). Notably, daytime SOA had a higher oxidation state, implying the importance of photooxidation in producing highly oxidized OA. This may be because of the high temperature at daytime and a species may require a lower volatility (hereby more oxygenated) to be in condensed phase than at night.

354
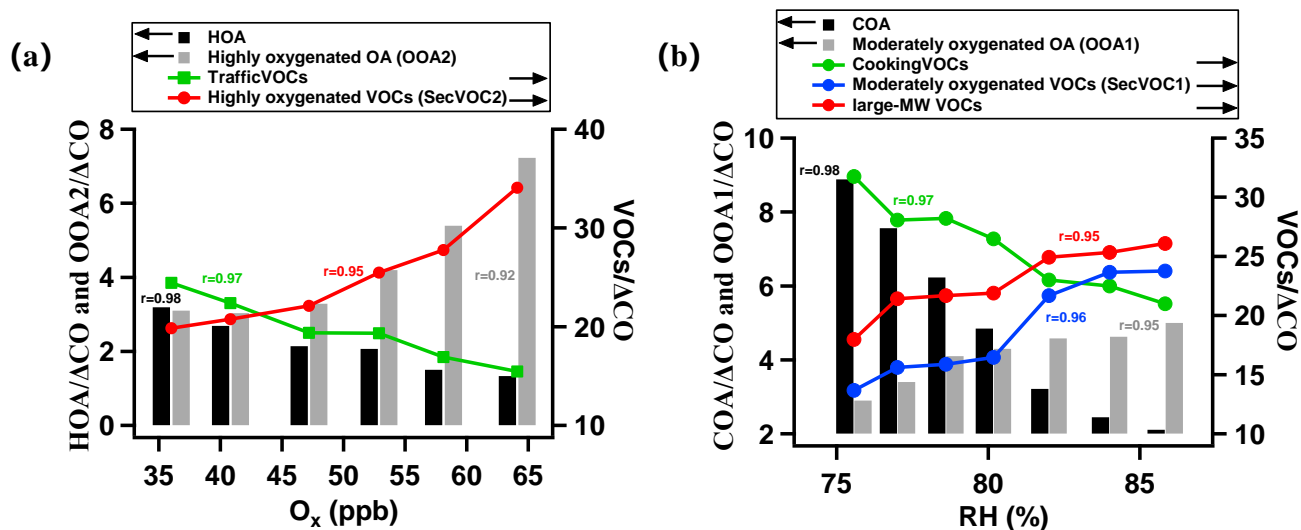
Figure 5. Daytime and nighttime evolution of key species against O$_x$ and RH respectively. (a) Daytime oxidation showing the primary emissions of traffic source in gas and aerosol phases including HOA, traffic VOCs; and secondary products including SecVOC2 and OOA2, with concentrations all normalized by ΔCO. (b) Nighttime oxidation showing the primary emissions of cooking source in gas and aerosol phases including COA and cooking VOCs; and secondary products including SecVOC1, large-MW VOC and OOA1, with concentrations all normalized by ΔCO.

4 Conclusion

In this study, organic gases and aerosols were concurrently characterized through online mass spectrometers at a megacity in central China. Through the factorization analysis on the organic mass spectra, two principal sources-the traffic and cooking sources were identified for both aerosol and gas phases, hereby the reacted and produced species between phases were interlinked. We observed clear evidence of daytime and nighttime oxidation of source-attributed OA and VOCs. Daytime photooxidation caused 60 % decrease of primary aerosol and 40 % of primary VOCs reduction for traffic sources, producing oxygenated SecVOCs by a factor of 1.7 and OOA by a factor of 2.5, in a 6 hours photochemical ageing. Nocturnal ageing caused a reduction of primary OA (by 77 %) and primary VOCs (by 35 %) from cooking sources, producing oxygenated VOCs and OOA by a factor of 1.4 and 1.7, respectively. In particular, larger molecular IVOCs produced (by a factor of 1.7) at night may importantly contribute to the OOA. This implies primary species in aerosol and gas phases both contribute to the production of OOA. A higher oxidation state of OOA from daytime photooxidation was found than nighttime, suggesting different compositions of produced OOA modulated by solar radiation and moisture, respectively. Vehicle and cooking emissions are the major contributors of organic aerosols in urban areas, especially in megacities. These results provide direct observations about the reaction rate for primary precursors and production rate for secondary aerosols, as influenced by primary sources and meteorological conditions. The environmental policy making should therefore consider the respective primary sources and ageing mechanisms for local and regional atmospheric

377 environmental problems. The particular regulation should be placed to avoid the formation of daytime highly-oxidized

378 species when high solar radiation, which may contribute to the reactive oxygen species and exert adverse health impacts

379 (Tao et al., 2003; Verma et al., 2009).

Data availability

381   The data in this study are available from the corresponding author upon request.

Author contribution

383   DL, SK, and SL led and designed the study. SL, YW, HZ, YC, SZ and DH set up and conducted the experiment. SL,

384 DL, YW, KH, XJ and SD contributed to the data analysis. QL, DZ, JS provided technical support and assistance. SL and DL

385 wrote the manuscript. All authors read and approved the final manuscript.

Competing interests

387   The authors declare no competing interests.

Acknowledgments

389   This work was supported by the National Natural Science Foundation of China (Grant Nos. 42175116, 41875167), the

390 National Key R&D programme of China (2019YFC0214703).

391

References

393 Adler, G., Flores, J. M., Abo Riziq, A., Borrmann, S., and Rudich, Y.: Chemical, physical, and optical evolution of biomass burning

394   aerosols: a case study, Atmos. Chem. Phys., 11, 1491-1503, https://doi.org/10.5194/acp-11-1491-2011, 2011.

395 Aiken, A., Salcedo, D., Cubison, M., Huffman, J., DeCarlo, P., Ulbrich, I., Docherty, K., Sueper, D., Kimmel, J., Worsnop, D., A, T., M,

396   N., Stone, E., Schauer, J., Volkamer, R., Fortner, E., de Foy, B., Wang, J., Laskin, A., and Jimenez, J.: Mexico City Aerosol Analysis

397   During Milagro Using High Resolution Aerosol Mass Spectrometry at the Urban Supersite (T0) - Part 1: Fine Particle Composition

398   and Organic Source Apportionment, Atmos. Chem. Phys., 9, 6633-6653, https://doi.org/10.5194/acpd-9-8377-2009, 2009.

399 Allan, J. D., Williams, P., Morgan, W., Martin, C., Flynn, M., Lee, J., Nemitz, E., Phillips, G., Gallagher, M., and Coe, H.: Contributions

400   from transport, solid fuel burning and cooking to primary organic aerosols in two UK cities, Atmos. Chem. Phys., 10, 647-668,

401   https://doi.org/10.5194/acp-10-647-2010, 2010.

402 Bruns, E. A., El Haddad, I., Slowik, J. G., Kilic, D., Klein, F., Baltensperger, U., and Prévôt, A. S. H.: Identification of significant

403   precursor gases of secondary organic aerosols from residential wood combustion, Sci. Rep., 6, 1-9, https://doi.org/10.1038/srep27881,

404   2016.

405 Cai, C., Geng, F., Tie, X., Yu, Q., and An, J.: Characteristics and source apportionment of VOCs measured in Shanghai, China, Atmos.

406   Environ., 44, 5005-5014, https://doi.org/10.1016/j.atmosenv.2010.07.059, 2010.

407 Canagaratna, M. R., Jayne, J. T., Jimenez, J. L., Allan, J. D., Alfarra, M. R., Zhang, Q., Onasch, T. B., Drewnick, F., Coe, H.,

408   Middlebrook, A., Delia, A., Williams, L. R., Trimborn, A. M., Northway, M. J., DeCarlo, P. F., Kolb, C. E., Davidovits, P., and

409   Worsnop, D. R.: Chemical and microphysical characterization of ambient aerosols with the aerodyne aerosol mass spectrometer,

410   Mass Spectrom Rev., 26, 185-222, https://doi.org/10.1002/mas.20115, 2007.

411 Canagaratna, M. R., Jimenez, J. L., Kroll, J. H., Chen, Q., Kessler, S. H., Massoli, P., Hildebrandt Ruiz, L., Fortner, E., Williams, L. R.,

412   Wilson, K. R., Surratt, J. D., Donahue, N. M., Jayne, J. T., and Worsnop, D. R.: Elemental ratio measurements of organic compounds

413   using aerosol mass spectrometry: characterization, improved calibration, and implications, Atmos. Chem. Phys., 15, 253-272,

414   https://doi.org/10.5194/acp-15-253-2015, 2015.

415 Cappellin, L., Karl, T., Probst, M., Ismailova, O., Winkler, P. M., Soukoulis, C., Aprea, E., Mark, T. D., Gasperi, F., and Biasioli, F.: On

416   quantitative determination of volatile organic compound concentrations using proton transfer reaction time-of-flight mass

417   spectrometry, Environ. Sci. Technol., 46, 2283-2290, https://doi.org/10.1021/es203985t, 2012.

418 Chen, T., Liu, J., Ma, Q., Chu, B., Zhang, P., Ma, J., Liu, Y., Zhong, C., Liu, P., Wang, Y., Mu, Y., and He, H.: Measurement report:

419   Effects of photochemical aging on the formation and evolution of summertime secondary aerosol in Beijing, Atmos. Chem. Phys., 21,

420   1341-1356, https://doi.org/10.5194/acp-21-1341-2021, 2021.

421 Claeys, M., Graham, B., Vas, G., Wu, W., Vermeylen, R., Pashynska, V., Cafmeyer, J., Cuyon, P., Andreae, M. O., and Artaxo, P.:

422   Formation of secondary organic aerosols through photooxidation of isoprene, Science, 303, 1173-1176,

423   https://doi.org/10.1126/science.1092805, 2004.

424 Clark, C. H., Kacarab, M., Nakao, S., Asa-Awuku, A., Sato, K., and Cocker III, D. R.: Temperature effects on secondary organic aerosol

425   (SOA) from the dark ozonolysis and photo-oxidation of isoprene, Environ. Sci. Technol., 50, 5564-5571,

426   https://doi.org/10.1021/acs.est.5b05524, 2016.

427 Decarlo, P. F., Kimmel, J. R., Trimborn, A., Northway, M. J., Jayne, J. T., Aiken, A. C., Gonin, M., Fuhrer, K., Horvath, T., and Docherty,

428   K. S.: Field-deployable, high-resolution, time-of-flight aerosol mass spectrometer, Anal. Chem., 78, 8281-8289,

429   https://doi.org/10.1021/ac061249n, 2006.

430 Decarlo, P. F., Ulbrich, I. M., Crounse, J., Foy, B. D., Dunlea, E. J., Aiken, A. C., Knapp, D., Weinheimer, A. J., Campos, T., and

431   Wennberg, P. O.: Investigation of the sources and processing of organic aerosol over the Central Mexican Plateau from aircraft

432   measurements during MILAGRO, Atmos. Chem. Phys., 10, 5257–5280, https://doi.org/10.5194/acp-10-5257-2010, 2010.

433 Donahue, N. M., Robinson, A. L., Stanier, C. O., and Pandis, S. N.: Coupled partitioning, dilution, and chemical aging of semivolatile

434   organics, Environ. Sci. Technol., 40, 2635-2643, https://doi.org/10.1021/es052297c, 2006.

435 Draxler, R. and Hess, G.: Description of the HYSPLIT_4 modelling system, NOAA Tech. Mem. ERL ARL-224, 1997.

436 Fang, H., Huang, X., Zhang, Y., Pei, C., Huang, Z., Wang, Y., Chen, Y., Yan, J., Zeng, J., Xiao, S., Luo, S., Li, S., Wang, J., Zhu, M., Fu,

437   X., Wu, Z., Zhang, R., Song, W., Zhang, G., Hu, W., Tang, M., Ding, X., Bi, X., and Wang, X.: Measurement report: Emissions of

438   intermediate-volatility organic compounds from vehicles under real-world driving conditions in an urban tunnel, Atmos. Chem.

439   Phys., 21, 10005-10013, https://doi.org/10.5194/acp-21-10005-2021, 2021.

440 Gkatzelis, G. I., Coggon, M. M., McDonald, B. C., Peischl, J., Gilman, J. B., Aikin, K. C., Robinson, M. A., Canonaco, F., Prevot, A. S.

441   H., Trainer, M., and Warneke, C.: Observations confirm that volatile chemical products are a major source of petrochemical

442   emissions in US cities, Environ. Sci. Technol., 55, 4332-4343, https://doi.org/10.1021/acs.est.0c05471, 2021.

443 Goldstein, A. H. and Galbally, I. E.: Known and Unexplored Organic Constituents in the Earth's Atmosphere, Environ. Sci. Technol., 41,

444   1514-1521, https://doi.org/10.1021/es072476p, 2007.

445 Gouw, J. D. and Jimenez, J. L.: Organic aerosols in the earth's atmosphere, Environ. Sci. Technol., 43, 7614-7618,
446   https://doi.org/10.1021/es9006004, 2009.

447 Gu, C., Wang, S., Zhu, J., Wu, S., Duan, Y., Gao, S., and Zhou, B.: Investigation on the urban ambient isoprene and its oxidation
448   processes, Atmos. Environ., 270, 118870, https://doi.org/10.1016/j.atmosenv.2021.118870, 2021.

449 Guo, J., Zhou, S., Cai, M., Zhao, J., Song, W., Zhao, W., Hu, W., Sun, Y., He, Y., Yang, C., Xu, X., Zhang, Z., Cheng, P., Fan, Q., Hang,
450   J., Fan, S., Wang, X., and Wang, X.: Characterization of submicron particles by time-of-flight aerosol chemical speciation monitor
451   (ToF-ACSM) during wintertime: aerosol composition, sources, and chemical processes in Guangzhou, China, Atmos. Chem. Phys.,
452   20, 7595-7615, https://doi.org/10.5194/acp-20-7595-2020, 2020.

453 Hallquist, M., Wenger, J. C., Baltensperger, U., Rudich, Y., Simpson, D., Claeys, M., Dommen, J., Donahue, N. M., George, C.,
454   Goldstein, A. H., Hamilton, J. F., Herrmann, H., Hoffmann, T., Iinuma, Y., Jang, M., Jenkin, M. E., Jimenez, J. L., Kiendler-Scharr,
455   A., Maenhaut, W., Mcfiggans, G., Mentel, T. F., Monod, A., Prevot, A. S. H., Seinfeld, J. H., Surratt, J. D., Szmigielski, R., and
456   Wildt, J.: The formation, properties and impact of secondary organic aerosol: current and emerging issues, Atmos. Chem. Phys., 9,
457   5155-5236, https://doi.org/10.5194/acp-9-5155-2009, 2009.

458 Hartikainen, A., Yli-Pirilä, P., Tiitta, P., Leskinen, A., Kortelainen, M., Orasche, J., Schnelle-Kreis, J., Lehtinen, K., Zimmermann, R.,
459   Jokiniemi, J., and Sippula, O.: Volatile organic compounds from logwood combustion: Emissions and transformation under dark and
460   photochemical aging conditions in a smog chamber, Environ. Sci. Technol., 52, 4979–4988, https://doi.org/10.1021/acs.est.7b06269,
461   2018.

462 Hatch, L. E., Yokelson, R. J., Stockwell, C. E., Veres, P. R., Simpson, I. J., Blake, D. R., Orlando, J. J., and Barsanti, K. C.: Multi-
463   instrument comparison and compilation of non-methane organic gas emissions from biomass burning and implications for smoke-
464   derived secondary organic aerosol precursors, Atmos. Chem. Phys., 17, 1471-1489, https://doi.org/10.5194/acp-17-1471-2017, 2017.

465 Hayes, P. L., Ortega, A. M., Cubison, M. J., Froyd, K. D., Zhao, Y., Cliff, S. S., Hu, W. W., Toohey, D. W., Flynn, J. H., Lefer, B. L.,
466   Grossberg, N., Alvarez, S., Rappenglück, B., Taylor, J. W., Allan, J. D., Holloway, J. S., Gilman, J. B., Kuster, W. C., de Gouw, J.
467   A., Massoli, P., Zhang, X., Liu, J., Weber, R. J., Corrigan, A. L., Russell, L. M., Isaacman, G., Worton, D. R., Kreisberg, N. M.,
468   Goldstein, A. H., Thalman, R., Waxman, E. M., Volkamer, R., Lin, Y. H., Surratt, J. D., Kleindienst, T. E., Offenberg, J. H.,
469   Dusanter, S., Griffith, S., Stevens, P. S., Brioude, J., Angevine, W. M., and Jimenez, J. L.: Organic aerosol composition and sources
470   in Pasadena, California, during the 2010 CalNex campaign, J. Geophys. Res.-Atmos., 118, 9233-9257,
471   https://doi.org/10.1002/jgrd.50530, 2013.

472 Heald, C. L., Jacob, D. J., Park, R. J., Russell, L. M., Huebert, B. J., Seinfeld, J. H., Liao, H., and Weber, R. J.: A large organic aerosol
473   source in the free troposphere missing from current models, Geophys. Res. Lett., 32, https://doi.org/10.1029/2005gl023831, 2005.

474 Hu, D., Liu, D., Kong, S., Zhao, D., Wu, Y., Li, S., Ding, S., Zheng, S., Cheng, Y., Hu, K., Deng, Z., Wu, Y., Tian, P., Liu, Q., Huang, M.,
475   and Ding, D.: Direct quantification of droplet activation of ambient black carbon under water supersaturation, J. Geophys. Res.-
476   Atmos., 126, https://doi.org/10.1029/2021jd034649, 2021.

477 Hu, W., Hu, M., Hu, W.-W., Zheng, J., Chen, C., Wu, Y., and Guo, S.: Seasonal variations in high time-resolved chemical compositions,
478   sources, and evolution of atmospheric submicron aerosols in the megacity Beijing, Atmos. Chem. Phys., 17, 9979-10000,
479   https://doi.org/10.5194/acp-17-9979-2017, 2017.

480 Hu, W., Hu, M., Hu, W., Jimenez, J., Yuan, B., Chen, W., Wang, M., Wu, Y., Chen, C., Wang, Z., Peng, J., Zeng, L., and Shao, M.:
481   Chemical composition, sources, and aging process of submicron aerosols in Beijing: Contrast between summer and winter, Journal of
482   Geophysical Research: Atmospheres, 121, 1955-1977, https://doi.org/10.1002/2015JD024020, 2016.

483 Hu, W. W., Hu, M., Yuan, B., Jimenez, J. L., Tang, Q., Peng, J. F., Hu, W., Shao, M., Wang, M., Zeng, L. M., Wu, Y. S., Gong, Z. H.,
484   Huang, X. F., and He, L. Y.: Insights on organic aerosol aging and the influence of coal combustion at a regional receptor site of
485   central eastern China, Atmos. Chem. Phys., 13, 10095-10112, https://doi.org/10.5194/acp-13-10095-2013, 2013.

486 Huang, L., Wang, Q., Wang, Y., Emery, C., Zhu, A., Zhu, Y., Yin, S., Yarwood, G., Zhang, K., and Li, L.: Simulation of secondary
487   organic aerosol over the Yangtze River Delta region: The impacts from the emissions of intermediate volatility organic compounds
488   and the SOA modeling framework, Atmos. Environ., 246, 118079, https://doi.org/10.1016/j.atmosenv.2020.118079, 2021.

489 Huang, R. J., Zhang, Y., Bozzetti, C., Ho, K. F., Cao, J. J., Han, Y., Daellenbach, K. R., Slowik, J. G., Platt, S. M., Canonaco, F., Zotter,
490   P., Wolf, R., Pieber, S. M., Bruns, E. A., Crippa, M., Ciarelli, G., Piazzalunga, A., Schwikowski, M., Abbaszade, G., Schnelle-Kreis,
491   J., Zimmermann, R., An, Z., Szidat, S., Baltensperger, U., El Haddad, I., and Prevot, A. S.: High secondary aerosol contribution to
492   particulate pollution during haze events in China, Nature, 514, 218-222, https://doi.org/10.1038/nature13774, 2014.

493 Huang, X. F., He, L. Y., Hu, M., Canagaratna, M. R., Sun, Y., Zhang, Q., Zhu, T., Xue, L., Zeng, L. W., Liu, X. G., Zhang, Y. H., Jayne,
494   J. T., Ng, N. L., and Worsnop, D. R.: Highly time-resolved chemical characterization of atmospheric submicron particles during 2008
495   Beijing Olympic Games using an Aerodyne High-Resolution Aerosol Mass Spectrometer, Atmos. Chem. Phys., 10, 8933-8945,
496   https://doi.org/10.5194/acp-10-8933-2010, 2010.

497 Jayne, J. T., Leard, D. C., Zhang, X., Davidovits, P., Smith, K. A., Kolb, C. E., and Worsnop, D. R.: Development of an aerosol mass
498   spectrometer for size and composition analysis of submicron particles, Aerosol Sci. Tech., 33, 49-70,
499   https://doi.org/10.1080/027868200410840, 2000.

500 Jokinen, T., Berndt, T., Makkonen, R., Kerminen, V. M., and Sipil, M.: Production of extremely low volatile organic compounds from
501   biogenic emissions: Measured yields and atmospheric implications, P. Natl. Acad. Sci. USA, 112, 7123-7128,
502   https://doi.org/10.1073/pnas.1423977112, 2015.

503 Klein, F., Platt, S. M., Farren, N. J., Detournay, A., Bruns, E. A., Bozzetti, C., Daellenbach, K. R., Kilic, D., Kumar, N. K., Pieber, S. M.,
504   Slowik, J. G., Temime-Roussel, B., Marchand, N., Hamilton, J. F., Baltensperger, U., Prevot, A. S., and El Haddad, I.:
505   Characterization of gas-phase organics using proton transfer reaction time-of-flight mass spectrometry: cooking emissions, Environ.
506   Sci. Technol., 50, 1243-1250, https://doi.org/10.1021/acs.est.5b04618, 2016.

507 Kroll, J. and Seinfeld, J.: Chemistry of secondary organic aerosol: Formation and evolution of low-volatility organics in the atmosphere,
508   Atmos. Environ., 42, 3593-3624, https://doi.org/10.1016/j.atmosenv.2008.01.003, 2008.

509 Laborde, M., Schnaiter, M., Linke, C., Saathoff, H., Naumann, K.-H., Möhler, O., Berlenz, S., Wagner, U., Taylor, J., Liu, D., Flynn, M.,
510   Allan, J., Coe, H., Heimerl, K., Dahlkötter, F., Weinzierl, B., Wollny, A. G., Zanatta, M., Cozic, J., and Gysel, M.: Single Particle
511   Soot Photometer intercomparison at the AIDA chamber, Atmos. Meas. Tech., 5, 3077-3097, https://doi.org/10.5194/amt-5-3077-
512   2012, 2012.

513 Lanz, V. A., Alfarra, M. R., Baltensperger, U., Buchmann, B., Hueglin, C., Szidat, S., Wehrli, M. N., Wacker, L., Weimer, S., and Caseiro,
514   A.: Source attribution of submicron organic aerosols during wintertime inversions by advanced factor analysis of aerosol mass
515   spectra, Environ. Sci. Technol., 42, 214-220, https://doi.org/10.1021/es0707207, 2008.

516 Li, J., Cao, L., Gao, W., He, L., Yan, Y., He, Y., Pan, Y., Ji, D., Liu, Z., and Wang, Y.: Seasonal variations in the highly time-resolved
517   aerosol composition, sources and chemical processes of background submicron particles in the North China Plain, Atmos. Chem.
518   Phys., 21, 4521-4539, https://doi.org/10.5194/acp-21-4521-2021, 2021a.

519 Li, S., Liu, D., Hu, D., Kong, S., Wu, Y., Ding, S., Cheng, Y., Qiu, H., Zheng, S., Yan, Q., Zheng, H., Hu, K., Zhang, J., Zhao, D., Liu, Q.,
520   Sheng, J., Ye, J., He, H., and Ding, D.: Evolution of organic aerosol from wood smoke influenced by burning phase and solar
521   radiation, J. Geophys. Res.-Atmos., 126, https://doi.org/10.1029/2021JD034534, 2021b.

522 Li, Y., Pöschl, U., and Shiraiwa, M.: Molecular corridors and parameterizations of volatility in the chemical evolution of organic aerosols,
523   Atmos. Chem. Phys., 16, 3327-3344, https://doi.org/10.5194/acp-16-3327-2016, 2016.

524 Lin, G., Penner, J. E., Sillman, S., Taraborrelli, D., and Lelieveld, J.: Global modeling of SOA formation from dicarbonyls, epoxides,
525   organic nitrates and peroxides, Atmos. Chem. Phys., 12, 4743-4774, https://doi.org/10.5194/acp-12-4743-2012, 2012.

526 Lin, Y. H., Zhang, H., Pye, H. O., Zhang, Z., Marth, W. J., Park, S., Arashiro, M., Cui, T., Budisulistiorini, S. H., Sexton, K. G., Vizuete,
527   W., Xie, Y., Luecken, D. J., Piletic, I. R., Edney, E. O., Bartolotti, L. J., Gold, A., and Surratt, J. D.: Epoxide as a precursor to
528   secondary organic aerosol formation from isoprene photooxidation in the presence of nitrogen oxides, P. Natl. Acad. Sci. USA, 110,
529   6718-6723, https://doi.org/10.1073/pnas.1221150110, 2013.

530 Liu, D., Flynn, M., Gysel, M., Targino, A., Crawford, I., Bower, K., Choularton, T., Jurányi, Z., Steinbacher, M., Hüglin, C., Curtius, J.,
531   Kampus, M., Petzold, A., Weingartner, E., and Baltensperger, U.: Single particle characterization of black carbon aerosols at a
532   tropospheric alpine site in Switzerland, Atmos. Chem. Phys., 10, 7389-7407, https://doi.org/10.5194/acpd-10-8765-2010, 2010.

533 Liu, T., Wang, Z., Huang, D. D., Wang, X., and Chan, C. K.: Significant production of secondary organic aerosol from emissions of
534   heated cooking oils, Environ. Sci. Technol. Lett., 5, 32-37, https://doi.org/10.1021/acs.estlett.7b00530, 2017.

535 Middlebrook, A. M., Bahreini, R., Jimenez, J. L., and Canagaratna, M. R.: Evaluation of composition-dependent collection efficiencies for
536   the aerodyne aerosol mass spectrometer using field data, Aerosol Sci. Tech., 46, 258-271,
537   https://doi.org/10.1080/02786826.2011.620041, 2012.

538 Mohr, C., DeCarlo, P. F., Heringa, M. F., Chirico, R., Slowik, J. G., Richter, R., Reche, C., Alastuey, A., Querol, X., Seco, R., Peñuelas,
539   J., Jiménez, J. L., Crippa, M., Zimmermann, R., Baltensperger, U., and Prévôt, A. S. H.: Identification and quantification of organic
540   aerosol from cooking and other sources in Barcelona using aerosol mass spectrometer data, Atmos. Chem. Phys., 12, 1649-1665,
541   https://doi.org/10.5194/acp-12-1649-2012, 2012.

542 Moody, J. L. and Galloway, J. N.: Quantifying the relationship between atmospheric transport and the chemical composition of
543   precipitation on Bermuda, Tellus B, 40, 463-479, https://doi.org/10.1111/j.1600-0889.1988.tb00117.x, 1988.

544 Morgan, W., Allan, J., Bower, K., Highwood, E., Liu, D., McMeeking, G., Northway, M., Williams, P., Krejci, R., and H, C.: Airborne
545   measurements of the spatial distribution of aerosol chemical composition across Europe and evolution of the organic fraction, Atmos.
546   Chem. Phys., 10, https://doi.org/10.5194/acpd-9-27215-2009, 2010.

547 Ng, N., Jimenez, J., Chhabra, P., Seinfeld, J., and Worsnop, D.: Changes in organic aerosol composition with aging inferred from aerosol
548   mass spectra, Atmos. Chem. Phys., 11, 6465-6474, https://doi.org/10.5194/acp-11-6465-2011, 2011a.

549 Ng, N. L., Canagaratna, M. R., Jimenez, I. L., Zhang, Q., Ulbrich, I. M., and Worsnop, D. R.: Real-time methods for estimating organic
550   component mass concentrations from aerosol mass spectrometer data, Environ. Sci. Technol., 45, 910-916,
551   https://doi.org/10.1021/es102951k, 2011b.

552 Ortiz-Montalvo, D. L., Hakkinen, S. A., Schwier, A. N., Lim, Y. B., McNeill, V. F., and Turpin, B. J.: Ammonium addition (and aerosol
553   pH) has a dramatic impact on the volatility and yield of glyoxal secondary organic aerosol, Environ. Sci. Technol., 48, 255-262,
554   https://doi.org/10.1021/es4035667, 2014.

555 Paatero, P. and Tapper, U.: Positive matrix factorization: A non-negative factor model with optimal utilization of error estimates of data
556   values, Environmetrics, 5, 111-126, https://doi.org/10.1002/env.3170050203, 1994.

Poschl, U.: Atmospheric aerosols: composition, transformation, climate and health effects, Angew. Chem. Int. Edit., 44, 7520-7540, https://doi.org/10.1002/anie.200501122, 2005.

Robinson, A. L., Donahue, N. M., Shrivastava, M. K., Weitkamp, E. A., Sage, A. M., Grieshop, A. P., Lane, T. E., Pierce, J. R., and Pandis, S. N.: Rethinking organic aerosols: semivolatile emissions and photochemical aging, Science, 315, 1259-1262, https://doi.org/10.1126/science.1133061, 2007.

Rogge, W. F., Hildemann, L. M., Mazurek, M. A., Cass, G. R., and Simoneit, B.: Sources of fine organic aerosol. 1. Charbroilers and meat cooking operations, Environ. Sci. Technol., 25, 1112-1125, https://doi.org/10.1021/es00018a015, 1991.

Sareen, N., Moussa, S. G., and McNeill, V. F.: Photochemical aging of light-absorbing secondary organic aerosol material, J. Phys. Chem. A., 117, 2987-2996, https://doi.org/10.1021/jp309413j, 2013.

Schwarz, J., Gao, R., Spackman, J. R., Watts, L., Thomson, D. S., Fahey, D., Ryerson, T., Peischl, J., Holloway, J., Trainer, M., Frost, G., Baynard, T., Lack, D., de Gouw, J., warneke, C., and Del Negro, L.: Measurement of the mixing state, mass, and optical size of individual black carbon particles in urban and biomass burning emissions, Geophys. Res. Lett., 35, L13810, https://doi.org/10.1029/2008GL033968, 2008.

Seinfeld, J., Bretherton, C., Carslaw, K., Coe, H., DeMott, P., Dunlea, E., Feingold, G., Ghan, S., Guenther, A., Kahn, R., Kraucunas, I., Kreidenweis, S., Molina, M., Nenes, A., Penner, J., Prather, K., Ramanathan, V., Ramaswamy, V., Rasch, P., and Wood, R.: Improving our fundamental understanding of the role of aerosol−cloud interactions in the climate system, P. Natl. Acad. Sci. USA, 113, 5781-5790, https://doi.org/10.1073/pnas.1514043113, 2016.

Shrivastava, M., Cappa, C. D., Fan, J., Goldstein, A. H., Guenther, A. B., Jimenez, J. L., Kuang, C., Laskin, A., Martin, S. T., Ng, N. L., Petaja, T., Pierce, J. R., Rasch, P. J., Roldin, P., Seinfeld, J. H., Shilling, J., Smith, J. N., Thornton, J. A., Volkamer, R., Wang, J., Worsnop, D. R., Zaveri, R. A., Zelenyuk, A., and Zhang, Q.: Recent advances in understanding secondary organic aerosol: Implications for global climate forcing, Rev. Geophy., 55, 509-559, https://doi.org/10.1002/2016rg000540, 2017.

Shrivastava, M., Easter, R. C., Liu, X., Zelenyuk, A., Singh, B., Zhang, K., Ma, P.-L., Chand, D., Ghan, S., Jimenez, J. L., Zhang, Q., Fast, J., Rasch, P. J., and Tiitta, P.: Global transformation and fate of SOA: Implications of low-volatility SOA and gas-phase fragmentation reactions, J. Geophys. Res.-Atmos., 120, 4169-4195, https://doi.org/10.1002/2014jd022563, 2015.

Slowik, J. G., Vlasenko, A., McGuire, M., Evans, G. J., and Abbatt, J. P. D.: Simultaneous factor analysis of organic particle and gas mass spectra: AMS and PTR-MS measurements at an urban site, Atmos. Chem. Phys., 10, 1969-1988, https://doi.org/10.5194/acp-10-1969-2010, 2010.

Sun, Y., Jiang, Q., Wang, Z., Fu, P., Li, J., Yang, T., and Yin, Y.: Investigation of the sources and evolution processes of severe haze pollution in Beijing in January 2013, J. Geophys. Res.-Atmos., 119, 4380-4398, https://doi.org/10.1002/2014jd021641, 2014.

Sun, Y. L., Zhang, Q., Schwab, J. J., Demerjian, K. L., Chen, W. N., Bae, M. S., Hung, H. M., Hogrefe, O., Frank, B., Rattigan, O. V., and Lin, Y. C.: Characterization of the sources and processes of organic and inorganic aerosols in New York city with a high-resolution time-of-flight aerosol mass apectrometer, Atmos. Chem. Phys., 11, 1581-1602, https://doi.org/10.5194/acp-11-1581-2011, 2011.

Tao, F., Gonzalez-Flecha, B., and Kobzik, L.: Reactive oxygen species in pulmonary inflammation by ambient particulates, Free Radical Bio. Med., 35, 327-340, https://doi.org/10.1016/S0891-5849(03)00280-6, 2003.

Ulbrich, I. M., Canagaratna, M. R., Zhang, Q., Worsnop, D. R., and Jimenez, J. L.: Interpretation of organic components from Positive Matrix Factorization of aerosol mass spectrometric data, Atmos. Chem. Phys., 9, 2891-2918, https://doi.org/10.5194/acp-9-2891-2009, 2009.

594 Verma, V., Ning, Z., Cho, A. K., Schauer, J. J., Shafer, M. M., and Sioutas, C.: Redox activity of urban quasi-ultrafine particles from
595   primary and secondary sources, Atmos. Environ., 43, 6360-6368, https://doi.org/10.1016/j.atmosenv.2009.09.019, 2009.

596 von Schneidemesser, E., Monks, P. S., Gros, V., Gauduin, J., and Sanchez, O.: How important is biogenic isoprene in an urban
597   environment? A study in London and Paris, Geophys. Res. Lett., 38, https://doi.org/10.1029/2011gl048647, 2011.

598 Wang, J., Ye, J., Liu, D., Wu, Y., Zhao, J., Xu, W., Xie, C., Shen, F., Zhang, J., Ohno, P. E., Qin, Y., Zhao, X., Martin, S. T., Lee, A. K.
599   Y., Fu, P., Jacob, D. J., Zhang, Q., Sun, Y., Chen, M., and Ge, X.: Characterization of submicron organic particles in Beijing during
600   summertime: comparison between SP-AMS and HR-AMS, Atmos. Chem. Phys., 20, 14091-14102, https://doi.org/10.5194/acp-20-
601   14091-2020, 2020a.

602 Wang, J., Ye, J., Zhang, Q., Zhao, J., Wu, Y., Li, J., Liu, D., Li, W., Zhang, Y., Wu, C., Xie, C., Qin, Y., Lei, Y., Huang, X., Guo, J., Liu,
603   P., Fu, P., Li, Y., Lee, H. C., Choi, H., Zhang, J., Liao, H., Chen, M., Sun, Y., Ge, X., Martin, S. T., and Jacob, D. J.: Aqueous
604   production of secondary organic aerosol from fossil-fuel emissions in winter Beijing haze, P. Natl. Acad. Sci. USA, 118,
605   https://doi.org/10.1073/pnas.2022179118, 2021.

606 Wang, L., Slowik, J. G., Tripathi, N., Bhattu, D., and Prévôt, A.: Source characterization of volatile organic compounds measured by
607   proton-transfer-reaction time-of-flight mass spectrometers in Delhi, India, Atmos. Chem. Phys., 20, 9753-9770,
608   https://doi.org/10.5194/acp-20-9753-2020, 2020b.

609 Wood, E. C., Canagaratna, M. R., Herndon, S. C., Onasch, T. B., Kolb, C. E., Worsnop, D. R., Kroll, J. H., Knighton, W. B., Seila, R.,
610   Zavala, M., Molina, L. T., DeCarlo, P. F., Jimenez, J. L., Weinheimer, A. J., Knapp, D. J., Jobson, B. T., Stutz, J., Kuster, W. C., and
611   Williams, E. J.: Investigation of the correlation between odd oxygen and secondary organic aerosol in Mexico City and Houston,
612   Atmos. Chem. Phys., 10, 8947-8968, https://doi.org/10.5194/acp-10-8947-2010, 2010.

613 Xu, J., Zhang, Q., Chen, M., Ge, X., Ren, J., and Qin, D.: Chemical composition, sources, and processes of urban aerosols during
614   summertime in northwest China: insights from high-resolution aerosol mass spectrometry, Atmos. Chem. Phys., 14, 12593-12611,
615   https://doi.org/10.5194/acp-14-12593-2014, 2014.

616 Xu, W., Sun, Y., Wang, Q., Zhao, J., Wang, J., Ge, X., Xie, C., Zhou, W., Du, W., Li, J., Fu, P., Wang, Z., Worsnop, D. R., and Coe, H.:
617   Changes in aerosol chemistry from 2014 to 2016 in winter in Beijing: Insights from high-resolution aerosol mass spectrometry, J.
618   Geophys. Res.-Atmos., 124, 1132-1147, https://doi.org/10.1029/2018jd029245, 2019.

619 Zhang, Q., Jimenez, J. L., Canagaratna, M. R., Allan, J. D., Coe, H., Ulbrich, I., Alfarra, M. R., Takami, A., Middlebrook, A. M., Sun, Y.
620   L., Dzepina, K., Dunlea, E., Docherty, K., DeCarlo, P. F., Salcedo, D., Onasch, T., Jayne, J. T., Miyoshi, T., Shimono, A.,
621   Hatakeyama, S., Takegawa, N., Kondo, Y., Schneider, J., Drewnick, F., Borrmann, S., Weimer, S., Demerjian, K., Williams, P.,
622   Bower, K., Bahreini, R., Cottrell, L., Griffin, R. J., Rautiainen, J., Sun, J. Y., Zhang, Y. M., and Worsnop, D. R.: Ubiquity and
623   dominance of oxygenated species in organic aerosols in anthropogenically-influenced Northern Hemisphere midlatitudes, Geophys.
624   Res. Lett., 34, https://doi.org/10.1029/2007gl029979, 2007.

625 Zhang, Z., Zhu, W., Hu, M., Wang, H., Chen, Z., Shen, R., Yu, Y., Tan, R., and Guo, S.: Secondary organic aerosol from typical Chinese
626   domestic cooking emissions, Environ. Sci. Technol. Lett., 8, 24-31, https://doi.org/10.1021/acs.estlett.0c00754, 2020.

627 Zhao, Y., Nguyen, N. T., Presto, A. A., Hennigan, C. J., May, A. A., and Robinson, A. L.: Intermediate volatility organic compound
628   emissions from on-road diesel vehicles: chemical composition, emission factors, and estimated secondary organic aerosol production,
629   Environ. Sci. Technol., 49, 11516-11526, https://doi.org/10.1021/acs.est.5b02841, 2015.

630 Zheng, H., Kong, S., Chen, N., Niu, Z., Zhang, Y., Jiang, S., Yan, Y., and Qi, S.: Source apportionment of volatile organic compounds:
631   Implications to reactivity, ozone formation, and secondary organic aerosol potential, Atmos. Res., 249, 105344,
632   https://doi.org/10.1016/j.atmosres.2020.105344, 2021.

633 Zheng, H., Kong, S., Chen, N., Yan, Y., Liu, D., Zhu, B., Xu, K., Cao, W., Ding, Q., Lan, B., Zhang, Z., Zheng, M., Fan, Z., Cheng, Y.,
634   Zheng, S., Yao, L., Bai, Y., Zhao, T., and Qi, S.: Significant changes in the chemical compositions and sources of $PM_{2.5}$ in Wuhan
635   since the city lockdown as COVID-19, Sci. Total. Environ., 739, 140000, https://doi.org/10.1016/j.scitotenv.2020.140000, 2020.

636 Zheng, H., Kong, S., Yan, Q., Wu, F., Cheng, Y., Zheng, S., Wu, J., Yang, G., Zheng, M., Tang, L., Yin, Y., Chen, K., Zhao, T., Liu, D.,
637   Li, S., Qi, S., Zhao, D., Zhang, T., Ruan, J., and Huang, M.: The impacts of pollution control measures on $PM_{2.5}$ reduction: Insights of
638   chemical composition, source variation and health risk, Atmos. Environ., 197, 103-117,
639   https://doi.org/10.1016/j.atmosenv.2018.10.023, 2019.

640 Zhou, X., Li, Z., Zhang, T., Wang, F., Wang, F., Tao, Y., Zhang, X., Wang, F., and Huang, J.: Volatile organic compounds in a typical
641   petrochemical industrialized valley city of northwest China based on high-resolution PTR-MS measurements: Characterization,
642   sources and chemical effects, Sci. Total. Environ., 671, 883-896, https://doi.org/10.1016/j.scitotenv.2019.03.283, 2019.

643 Zhu, W., Guo, S., Zhang, Z., Wang, H., Yu, Y., Chen, Z., Shen, R., Tan, R., Song, K., Liu, K., Tang, R., Liu, Y., Lou, S., Li, Y., Zhang,
644   W., Zhang, Z., Shuai, S., Xu, H., Li, S., Chen, Y., Hu, M., Canonaco, F., and Prévôt, A. S. H.: Mass spectral characterization of
645   secondary organic aerosol from urban cooking and vehicular sources, Atmos. Chem. Phys., 21, 15065-15079,
646   https://doi.org/10.5194/acp-21-15065-2021, 2021.

647